Eur. Phys. J. B **10**, 607–621 (1999)

THE EUROPEAN PHYSICAL JOURNAL B

EDP Sciences

Phase diagram of doped spin-Peierls systems

M. Fabrizio[1,2,3], R. Mélin[4,a], and J. Souletie[4]

[1] International School for Advanced Studies SISSA-ISAS, Via Beirut 2-4, 34013 Trieste, Italy
[2] Istituto Nazionale di Fisica della Materia INFM
[3] International Centre for Theoretical Physics, Strada Costiera 11, 34014 Trieste, Italy
[4] Centre de Recherches sur les Très Basses Températures (CRTBT)[b], CNRS, BP 166, 38042 Grenoble Cedex 9, France

Received 8 July 1998 and Received in final form 16 February 1999

Abstract. The phase diagram of a model describing doped $CuGeO_3$ is derived. The model emphasizes the role of local moments released by the impurities and randomly distributed inside the gaped singlet background. The phase diagram is investigated by two methods: (i) in a mean field treatment of the interchain coupling and (ii) in a real space decimation procedure in a two-dimensional model of randomly distributed moments. Both methods lead to similar results, in a qualitative agreement with experiments. In particular, a transition to an inhomogeneous Néel phase is obtained for arbitrary small doping. From the decimation procedure, we interpret this phase at very low doping as a *Griffith antiferromagnet*. Namely, it does not have a true long range order down to zero temperature. Nonetheless, large magnetically ordered clusters appear already at relatively high temperatures. This demonstrates the role of disorder in the theoretical description of doping in $CuGeO_3$. A detailed comparison with other approaches is also given.

PACS. 75.10.Jm Quantized spin models – 75.50.Ee Antiferromagnetics

1 Introduction

Spin-Peierls systems have been the subject of a renewed interest because of the discovery of several inorganic quasi-one-dimensional (Q1D) spin-Peierls compounds. A very well studied example is $CuGeO_3$. This Q1D compound made of weakly coupled CuO_2 chains has a spin-Peierls transition at $T_{SP} \simeq 14$ K [1], as revealed by diffraction measurements, showing a dimerization below T_{SP}, and by susceptibility data, which indicate the opening of a spin gap at T_{SP}.

$CuGeO_3$ can be doped in a controlled fashion, giving the unique opportunity to study the role of impurities in a spin-Peierls system. Doping is done in two different ways. One possibility is to directly affect the spin degrees of freedom within each CuO_2 chain by substituting some of the Cu atoms (whose spin is $S = 1/2$) with magnetic (Ni [2], which has $S = 1$, or Co [3], $S = 3/2$) or non-magnetic (Zn [4–6], Mg [7]) impurities. Another way is by substituting Ge with Si [8], which is expected to modify the strength of the exchange couplings among the magnetic ions. For all these compounds, even a small amount of doping strongly enhances the magnetic fluctuations, leading in most cases to a lower temperature Néel phase coexisting with the Peierls's distorted phase. For instance, in 0.3% Si-doped compounds, free spins are released which contribute with a Curie-like behavior below $T_{SP} \simeq 12.5$ K (which is slightly reduced with respect to the undoped sample), and finally get frozen below the Néel temperature $T_N \simeq 0.95$ K [9]. The same behavior has been reported in a 2% Zn-doped compound, where magnetization measurements can be interpreted as if approximately one spin-1/2 per Zn atom is released [10]. In all cases but Co-doped samples [11], the low doping $x < 1\%$ phase diagram seems to have universal features [12]: T_{SP} decreases almost linearly with x, while no critical concentration for the appearance of the Néel phase has till now been revealed down to the lowest accessible impurity concentrations (*e.g.* 0.12% Zn for which $T_N \simeq 0.025$ K [13]).

At larger doping, the situation is still not fully established. However, most of the data indicate that over some critical x_c, the spin-Peierls long-range order disappears, although short-range correlations seem to persist. For Mg-doped samples, it is claimed that at $x_c \simeq 2.3\%$ a first order phase transition takes place which is signaled by a jump of T_N [7].

Manabe *et al.* [13] have reported an antiferromagnetic (AF) ordering with Zn concentrations as low as 0.11%. Their analysis of the variation of the Néel temperature *versus* doping concentration has shown the absence of a critical doping concentration for AF ordering at zero temperature ($x_c = 0$). The goal of the present article is to understand this onset of long range AF order at such low doping. This experimental observation questions

[a] e-mail: melin@labs.polycnrs-gre.fr
[b] CNRS UPR 5001, Laboratoire conventionné avec l'Université Joseph Fourier

the validity of existing theories in a much more drastic way than the coexistence of AF order and dimerization.

Several distinct theories describe this coexistence of dimerization and antiferromagnetism. Fukuyama *et al.* [14] first proposed a model showing that the two orders can coexist, and another model was proposed by Mostovoy *et al.* [15]. Two of the present authors have proposed another model for the coexistence of AF ordering and dimerization [16,17]. All these theories successfully describe the coexistence of dimerization and AF order upon doping, and they also show that the effect of doping amounts to generate states inside the Spin-Peierls gap, in agreement with susceptibility experiments (for example [13]). A similar behavior is reported in spin-ladder systems, which, in spite of having a large spin gap, undergo a Néel transition upon very small doping. For instance $SrCu_2O_3$, with a spin gap of $\sim$ 400 K, has a finite $T_N \simeq 3$ K already at 1% Zn doping [18]. In these ladder compounds the low energy spin excitations induced by doping have also been revealed by a finite specific heat coefficient [18].

In their article, Manabe *et al.* pointed out that one energy scale emerging from our model (denoted by T_*, see Sects. 2.2 and 3 for its definition) was many orders of magnitude lower than the Néel temperature (for instance at $x = 0.1\%$, $T_* \simeq 4\times10^{-42}$ K whereas $T_N \simeq 20$ mK has been measured [13]). On the basis of the analysis of AF fluctuations in the 1D model, we already suggested [16,17] that this apparent inconsistence can be avoided if one makes a proper treatment of disorder averaging. In the present article, we push further this analysis by estimating the Néel temperature in the presence of interchain coupling, which turns the quasi-long-range AF fluctuations of the 1D model into a longer range order. We prove by two different methods (a mean field treatment of the interchain coupling, and a decimation procedure of the 2D disordered problem) that the resulting Néel temperature has the right order of magnitude. Moreover, under both treatments, we show that there is no critical concentration for the establishment of AF order. As it was shown by Mostovoy *et al.*, this is not the case in their model, and we believe that this is not the case either in the approach by Fukuyama *et al.*, further extended by Yoshioka and Suzumura [19].

The paper is organized as follows. We introduce the model in Section 2, and discuss the experiments by Manabe *et al.* [13]. The problem of interchain coupling is first solved in Section 3 at the mean field level. Section 4 is devoted to the decimation approach that goes beyond the mean field treatment of interchain interactions, and is more relevant for the extremely low doping situation. The picture of Griffith-like antiferromagnetism emerges from this treatment: large AF correlated clusters are formed when the temperature is decreased below the spin-Peierls temperature, without infinite range ordering. A summary of our results is presented in Section 5 together with a comparison with the approaches by Mostovoy *et al.* [15], Fukuyama *et al.* [14], and Yoshioka and Suzumura [19]. We argue that these approaches would fail to properly describe the low doping behavior, whereas our description leads to AF ordering at infinitesimal doping. Since the analysis of the work by Fukuyama *et al.* is more technically involved, we have kept the qualitative features for the concluding section while the technical aspects are left for the appendices.

2 The model

2.1 Generation of spin-1/2 moments

We start by briefly describing our model. Let us consider the Hamiltonian of a dimerized Heisenberg model. Given the large anisotropy in the couplings (for instance [20])

$$|J_a| \simeq J_c/100 \ll J_b \simeq J_c/10 \ll J_c \simeq 10.6 \text{ meV}, \qquad (1)$$

where c is the chain axis, and a and b the two perpendicular directions, the Néel temperature is mainly determined by J_c and J_b. We therefore consider the Hamiltonian of a dimerized Heisenberg model in two dimensions,

$$J\sum_{n,i}\left(1+\delta(1)^{i+n}\right)\mathbf{S}_{n,i}\cdot\mathbf{S}_{n,i+1} + J_\perp\sum_{n,i}\mathbf{S}_{n,i}\cdot\mathbf{S}_{n+1,i}, \qquad (2)$$

where $J = J_c$, $J_\perp = J_b$, i labels the sites along the chain and n is the chain index. δ is the dimerization parameter which is staggered along the b axis. In reality, frustration has to be added to get a reasonable agreement with the spin susceptibility data above T_{SP} [21]. This can be accomplished by introducing for instance a (quite large) next nearest neighbor exchange $J' \sim 0.23 - 0.36J$, which can result both from next nearest neighbor Cu-Cu superexchange and from the lattice quantum fluctuations. However, this additional complication is neglected in our present analysis.

When $\delta > 0$, each spin at an even site is coupled by a strong bond $J(1+\delta)$ to the spin at its left, and by a weak bond $J(1-\delta)$ to the spin at its right, both on the same chain. A finite gap between the singlet ground state and the lowest triplet excitation arises as soon as $\delta \neq 0$ and $J_\perp$ is less than a critical value which depends on δ. This should be the case of the pure $CuGeO_3$. We start by assuming that the most important effect of doping is that each impurity releases a free spin out of the dimerized singlet background. This behavior was anticipated in [22] on the basis of exact diagonalization of small-size systems, and in reference [16] by more qualitative arguments (see Fig. 1). Further numerical works have confirmed this picture [23,24], and have shown its robustness when more realistic assumptions are made, such as quantum phonons or coupling to a 3D lattice dimerization [25], or next-nearest-neighbor frustration [26]. The generation of spin-1/2 objects is most clearly seen for Zn or Mg doping and in the limit $J_\perp = 0$. As a first approximation, the non magnetic ion cuts the chain into two segments, *e.g.* one starting with a weak bond, the other ending with a strong bond. In the former segment, a free spin-1/2 moment will appear localized at the boundary. Even if we add a weak link across the non-magnetic ion, which couples the two end-spins of each segment, this free spin-1/2 moment still exists. An even

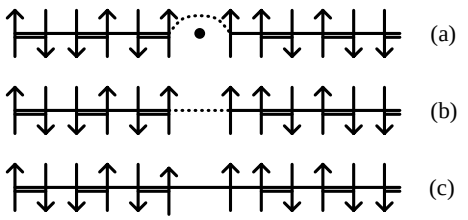

Fig. 1. Mapping of a segment with a non magnetic site to a squeezed segment, without this site. The double line represents a strong bond in the dimerized chain, *i.e.* $J(1+\delta)$, the single solid line a weak bond $J(1-\delta)$, while the dotted line is the weak link across the non magnetic site. Going from (b) to (c) we have assumed the weak link equal to the weak bond. Therefore the squeezed segment in (c) contains a domain wall, *i.e.* two consecutive weak links.

more transparent explanation is obtained by considering a ring of even number of sites. Since $\delta \neq 0$, the ground state is a singlet with a gap to the lowest $S = 1$ excitations. If a spin is removed, and a weak link across the empty site is added, the effective spin chain will now contain an odd number of spins 1/2. Hence the ground state will have $S = 1/2$, in spite of a finite gap to higher spin states. Moreover, since translational symmetry is broken, this $S = 1/2$ moment will be mostly localized around the weak link. Similarly, even if one spin 1/2 is substituted by a spin 1, modeling Ni doping, a free spin 1/2 moment is formed around the impurity. We also believe that the same situation holds with a finite $J_\perp$.

The case of Si-doping is less clear. Ge is supposed to influence the superexchange between the Cu's [27], increasing the antiferromagnetic superexchange with respect to the ferromagnetic indirect exchange, finally leading to a net $J > 0$. The smaller bond length of Si-O has likely the effect of reducing the antiferromagnetic superexchange by diminishing the angle Cu-O-Cu, thus inducing defects in the dimerized structure. In principle, a large reduction of that angle might even change the sign of the Cu-Cu exchange constant, leading to the formation of free spin-1 moments. Although we believe this is likely to occur, here we will limit our analysis to the simpler case of non magnetic ions substituting Cu.

We therefore take for granted the appearance of spin-1/2 moments upon doping, in the line of several numerical works (see *e.g.* Refs. [22–26]) and pursue the next step which is to build up the phase diagram of doped $CuGeO_3$ from these excitations. This cannot be done without including the effect of interactions between those spin-1/2 moments, which are central to our description.

As we argued, in such cases free spin-1/2 moments form around each impurity, showing up as low energy states inside the spin-Peierls gap, which, at very low doping, is almost unchanged. Therefore, we model the doped compounds as a two components system, where spins 1/2 are diluted inside a singlet background, characterized by a fixed gap between the singlet ground state and the first excited triplets. The virtual polarization of the singlet background provides an antiferromagnetic coupling between these spins. Since the dimerized state is gaped, this coupling decays exponentially with the distance between two spins over a length of the order of the spin-Peierls correlation length. For instance, let us consider two spins at a distance $\mathbf{r} = (n_x c, n_y b)$, n_x and n_y being positive integers, and c and b the lattice constants in the chain and perpendicular to the chain directions. Then, the exchange between these two impurity-released spins can be taken of the form

$$J(\mathbf{r}) \simeq -(-1)^{n_x+n_y} \Delta \exp\left(-\sqrt{\left(\frac{n_x}{\xi_x}\right)^2 + \left(\frac{n_y}{\xi_y}\right)^2}\right), \quad (3)$$

where Δ is the spin gap, $\xi_x = \xi_{\rm SP} \simeq 9-13$ [28] the correlation length in lattice constant units along the c-axis, while $\xi_y \sim \xi_{\rm SP} J_\perp/J \simeq 0.1\xi_{\rm SP}$, the correlation length along the b-axis. The oscillating factor in front takes into account the fact that the singlet background polarizes mostly in a staggered way, leading to a ferromagnetic exchange if the two spins are on the same sublattice and to an antiferromagnetic one in the opposite case. Since the impurities are located at random, replacing a fraction x of the magnetic sites, equation (3) defines a two-dimensional random Heisenberg model, which should properly describe the excitations at energies below the spin-Peierls gap.

The above two-component model looses its validity at larger doping, where the impurities start to affect the singlet background in a non negligible way. Nevertheless, we believe that at low doping it does capture the essential physics of the real system, giving a good description of the Néel transition. Below some temperature, these weakly coupled spins will tend to order antiferromagnetically. Moreover, they will also induce a staggered polarization on the singlet background, which does have a finite staggered susceptibility, in spite of an exponentially decaying uniform susceptibility. According to this scenario, the Néel phase would consist of spins antiferromagnetically ordered diluted in a partially polarized singlet background. The main problem is to get an estimate of the Néel transition temperature, which allows a direct comparison of the present model with the experimental phase diagram of $Cu_{1-x}Zn_xGeO_3$ [13], where it has been shown that zero temperature AF ordering occurs at an infinitesimal Zn concentration.

2.2 The typical energy scale T_* and the susceptibility experiments by Manabe et al. [13]

We first proceed by considering the extremely low doping susceptibility experiments by Manabe *et al.* [13], which, to our knowledge are the only available with Zn concentrations as low as 1.12×10^{-3}. As pointed out in reference [13], the Néel temperatures (see Tab. 1) are indeed much larger than the *typical energy scale* T_*, given by the Néel temperature of a regular array of equally spaced spin-1/2 moments with an exchange given by equation (3), which we may estimate by considering, instead of a random distribution, a regular distribution of the spins over the 2D lattice with a concentration x. The coupling along the c and b-axes are then $J_x = \Delta \exp(-l/\xi_x)$ and $J_y = \Delta \exp(-l/\xi_y)$,

Table 1. Parameters of the best fits of the susceptibility data by Manabe *et al.* to the forms (4) and (5) shown in Figure 2. The Néel temperature is also given, and is of the same order of magnitude as $J_{\rm imp}$ and θ. The values of $\langle\langle J\rangle\rangle$ (Eq. (8)) and T_* (Eq. (9)) are also given.

x (%)	$J_{\rm imp}$ (K)	$C_{\rm imp}$ (10^{-5} eum/g)	$C_{\rm SP}$ (10^{-5} eum/g)	θ (K)	C (10^{-5} eum/g)	$T_{\rm N}$ (K)	T_* (K)	$\langle\langle J\rangle\rangle$ (K)
0.112 (2)	0.0033	0.35	297	0.0035	0.35	0.027	10^{-42}	0.45
0.118 (2)	0.008	0.25	215	0.01	0.25	0.04	10^{-39}	0.47
0.213 (4)	0.04	0.7	242	0.035	0.69	0.14	10^{-21}	0.84
0.308 (6)	0.18	1.0	242	0.29	1.1	0.24	10^{-14}	1.2
0.491 (10)	0.58	1.6	229	1.34	2.14	0.7	10^{-8}	1.9

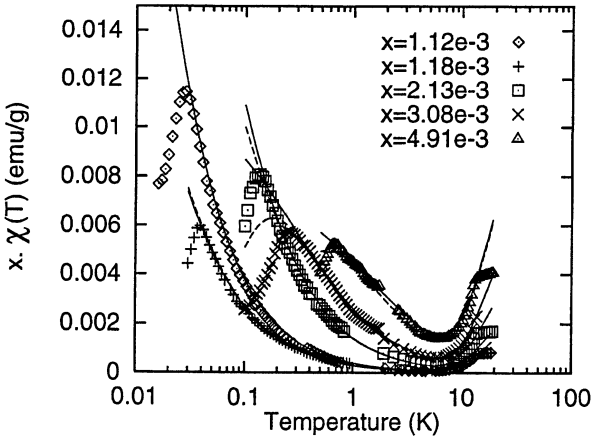

Fig. 2. Fit of the susceptibility experiments by Manabe *et al.* [13] to the Curie form (5) (solid lines) and to the form (4) (dashed lines). For clarity, we have multiplied the susceptibility by the concentration, so that all the concentration data are at the same scale at low temperature. Since the data provided to us by Manabe *et al.* were very dense in some temperature regions, we have "compressed" the data by averaging them over given bins. The parameters of the fits are shown in Table 1.

respectively, with $l = 1/\sqrt{x}$ the average distance between the spins. Hence, at low doping, the effective Heisenberg model describing the spins has a huge space anisotropy $J_x/J_y \sim \exp(-l/\xi_y) \ll 1$, implying that the scale controlling the Néel temperature is $T_* \sim J_y \sim 2\times 10^{-14}$ K if $x = 0.1\%$, which is far too small compared with the experimental values of the AF transition temperatures. The typical energy scale T_* can also be evaluated in the single chain version of our model, as recalled in Section 3. Experimentally, Manabe *et al.* [13] measure $0.027\ {\rm K} < T_{\rm N} < 0.7$ K in $CuGeO_3$, for concentration impurities ranging from 0.11% and 0.49% (see Tab. 1). A more accurate estimate of the characteristic exchange interaction can be made by fitting their data in the range $T_{\rm N} < T < T_{\rm SP}$.

We first decompose the susceptibility in the whole range between $T_{\rm N}$ and $T_{\rm SP}$ into two contributions:

$$\chi(T) = \frac{C_{\rm imp}}{T}\exp\left(-\frac{J_{\rm imp}}{T}\right) + \frac{C_{\rm SP}}{T}\exp\left(-\frac{\Delta}{T}\right), \qquad (4)$$

the first term corresponding to the low temperature contribution of Zn impurities, and the second term describing the higher temperature behavior of the susceptibility close to the spin-Peierls temperature. The energy scale involved in this contribution is the spin-Peierls gap $\Delta \simeq 44.7$ K. The fits for various impurity concentrations are shown in Figure 2, and are in a quite satisfactory agreement with experiments.

The three parameters $C_{\rm imp}$, $J_{\rm imp}$, $C_{\rm SP}$ are shown in Table 1. The energy scale $J_{\rm imp}$ involved in the fit of the impurity contribution sets the characteristic energy scale involved in the physics of impurity-released magnetic moments. As it can be seen in Table 1, $J_{\rm imp}$ is finite, which shows that the Zn-induced magnetic moments are interacting, consistent with our picture. Moreover, this energy scale is *not* of the order of the typical exchange T_*.

Alternatively, the susceptibility data in [13] can be fitted with the Curie-Weiss expression

$$\chi(T) = \frac{C}{\theta + T} + \frac{C_{\rm SP}}{T}\exp\left(-\frac{\Delta}{T}\right), \qquad (5)$$

a fit proposed in reference [9]. As it is visible in Figure 2, the form of the susceptibility also leads to a good description of the susceptibility for temperatures ranging between the Néel temperature and the spin-Peierls temperature. The parameters of the fits are shown in Table 1, and the energy scale θ involved in the fit (5) is again orders of magnitude larger than the typical exchange T_*. Both expressions (4, 5) have the same high temperature behavior in the limit $T \gg J, \theta$, and, in this regime, $\theta = J$. Once the two fits have been performed independently, we can check that these energy scales are indeed the same, as it is visible in Table 1, and comparable to the ordering temperature $T_{\rm N}$.

The reason why the Néel temperature is not of the order of T_*, but many orders of magnitude higher, is that, as a result of disorder in the spatial distribution of magnetic moments, clusters exist in the system with spins which are close to each other, being therefore strongly AF correlated. Once the interchain couplings will be included (Sects. 3 and 4), this will result in a Néel temperature many orders of magnitude larger than T_*.

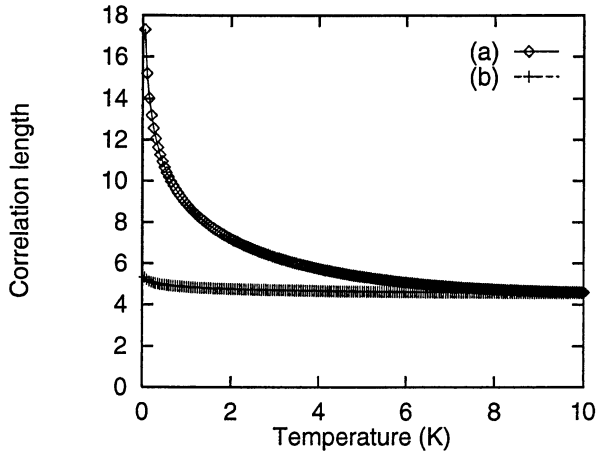

Fig. 3. Variations of the correlation length in the XX limit for $x = 0.3\%$ doping *versus* temperature, with $\xi_{\rm SP} = 9$ and $\Delta = 44.7$ K. (a) shows the variations of the correlation length of the disordered system and (b) the correlation length of the typical realization of disorder, namely, an array of equally spaced magnetic moments. The limiting value of the correlation length when $T \to T_{\rm SP}$ is $1/(n + 2/\xi_{\rm SP})$, the factor of 2 originating from the XX approximation.

3 Mean field theory of AF ordering

In this section we first recall (Sect. 3.1) the results obtained in 1D [16,17], discuss the energy scale T_* in the 1D model (Sect. 3.2), and present in Section 3.3 the extension to include the effect of the interchain coupling $J_\perp$. We take in this section as well as in the forthcoming Section 4 a spin-Peierls gap $\Delta = 44.7$ K [20], assumed to be independent on temperature. The spin-Peierls correlation length is $\xi_{\rm SP} = 9$ [28].

3.1 Physics of the 1D model

As shown in [16,17], a single chain does develop quasi-long range magnetic correlations at zero temperature, which we believe is the key point for understanding the establishment of AF ordering at arbitrarily low doping. More precisely, the correlation length $\xi(T)$ is found as the root of $f(y, \Gamma_T) + 1 = 0$, with $y = -1/\xi$, $\Gamma_T = \ln(\Delta/T)$, and

$$f(y,\Gamma) = \alpha \frac{f_0(y) - \alpha \tan(\alpha\Gamma)}{f_0(y)\tan(\alpha\Gamma) + \alpha},$$

where $\alpha = \xi_{\rm SP}\sqrt{-y(y+2x)}$, and $f_0(y) = \xi_{\rm SP}(y + x)$. The same solution holds in the XX limit, except that the correlation length is then found as the root of the equation $f(y, \Gamma_T) + 2 = 0$. The correlation length is compared in Figure 3 to that of an ordered array of magnetic moments separated by a distance of $1/x$ and interacting with an exchange $\Delta \exp(-1/x\xi_{\rm SP})$.

Finally, we will use latter the local staggered susceptibility $\chi_{\rm s}(T)$

$$\chi_{\rm s}(T) = x \left(\frac{1/\xi_{\rm SP}}{x \ln(\Delta/T) + 1/\xi_{\rm SP}} \right)^2 \frac{1}{4T} \cdot \qquad (6)$$

3.2 Energy scale T_*

The staggered spin-spin correlation function

$$\langle S^i(r) S^i(0) \rangle \sim (-1)^r \frac{{\rm e}^{-r/\xi(T)}}{r^2},$$

shows quasi-long-range AF fluctuations at low temperature, with the limiting behavior of the correlation length

$$\xi(T) \to \frac{2x\xi_{\rm SP}^2}{\pi^2} \ln^2\left(\frac{T}{\Delta}\right) \qquad (7)$$

valid at extremely low temperature $T < T_*$, in which case the system has crossed-over to the random singlet fixed point [17,29,30]. The distribution of the exchange constants is

$$P(J) = \frac{x\xi_{\rm SP}}{\Delta} \left(\frac{\Delta}{J}\right)^{1-x\xi_{\rm SP}} \theta(\Delta - J) \,.$$

This distribution $P(J)$ is such that the typical exchange constant (9), when $x\xi_{\rm SP} \ll 1$, is much smaller that the average exchange

$$\langle\langle J(r) \rangle\rangle = \Delta \frac{x\xi_{\rm SP}}{1 + x\xi_{\rm SP}} \cdot \qquad (8)$$

The energy scale T_* is defined by

$$T_* \simeq {\rm e}^{\langle\langle \log[J(r)] \rangle\rangle} = \Delta {\rm e}^{-1/(x\xi_{\rm SP})}, \qquad (9)$$

and is equal to the typical exchange constant among the spins. The symbol $\langle\langle \dots \rangle\rangle$ denotes a disorder average [31]. The definition of T_* in equation (9) in the 1D model is equivalent to the one we have introduced in Section 2.2 on the basis of a 2D modeling. Above this temperature, at which the correlation length is of the order of $1/x$ (the average distance between the impurities), $\xi(T)$ decreases with increasing temperature, approaching $\xi_{\rm SP}$ when $T \to \Delta$. As shown in Figure 3, at intermediate temperatures $T_* < T < T_{\rm SP}$ the AF correlation length is increased by disorder. Above T_*, the disordered chain takes advantage of rare fluctuations in which many spins get closer than the average distance $1/x$, thus forming AF correlated clusters due to the exponential dependence of the exchange (3) upon the distance.

The experimental values of the Néel temperature (see Tab. 1) are clearly of the order of the average exchange $\langle\langle J \rangle\rangle$, and not of the order of the typical exchange T_*. The same is true for the characteristic exchange $J_{\rm imp}$ in (4) and the (negative) Curie temperature θ in (5). The orders of magnitude of $J_{\rm imp}$ and θ obtained in Section 2.2 are in fact a proof of the relevance of disorder in the physics of the system.

3.3 Mean field treatment

We now include the effect of an interchain coupling $J_\perp \simeq 12$ K [20] under the form of a mean field treatment based

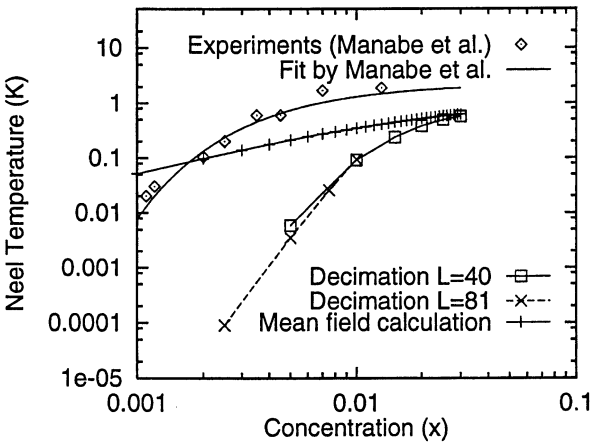

Fig. 4. Comparison between the experimental phase diagram by Manabe *et al.* [13] ($\Diamond$), our mean-field treatment (+) and the decimation results ($L = 40$: $\Box$; $L = 81$: $\times$). The fit to the experimental data is $A\exp(-B/x)$, with $A = 2.3$ K and $B = 5.7\times10^{-3}$. The mean field results (+) have been obtained with $\xi_{\rm SP} = 9c$ and $J_\perp = 12$ K. The decimation results have been calculated with sizes $L = 40$ ($\Box$) and $L = 81$ ($\times$), and correspond to an existence probability of 1/2. As it can be seen in this figure, both estimations of the Néel temperature at low doping are much larger than $T^* = \Delta\exp(-1/x\xi_{\rm SP})$ ($\simeq 10^{-47}$ K if $x = 0.1\%$). The experimental results as well as the results from the mean field treatment and the decimation procedure show no critical concentration. The mean field and decimation results have been obtained by using the known parameters (1) for $CuGeO_3$ as an input of the calculation, without adjusting any parameter.

on the 1D model proposed and analyzed in references [16,17]. As recalled in Section 3.1, the 1D version of our model does develop quasi-long-range AF fluctuations, which is the reason why AF order will be easily generated once an interchain coupling $J_\perp$ is taken into account. When the interchain exchange $J_\perp$ is switched on, a true Néel long range order might develop. The question whether the Néel order is a true long range order or a short range order will be discussed in more details in the light of the decimation calculation in Section 4. We look in the present section at the mean field response to a uniform staggered field, and therefore the Néel order is infinite ranged, which is not the case when the interchain coupling is included beyond the mean field treatment.

To get an estimate of the Néel temperature, we use the following mean-field like equation for $T_{\rm N}$:

$$J_\perp\chi_{\rm s}(T_{\rm N})\xi(T_{\rm N}) = 1, \tag{10}$$

where $\chi_{\rm s}(T)$ is the local staggered magnetic susceptibility (6), and $\xi(T)$ the correlation length drawn in Figure 3. The Néel temperature calculated *via* equation (10) is plotted in Figure 4 as a function of the impurity concentration x for different values of $J_\perp$. It is quite clear from the present calculation that the Néel temperature $T_{\rm N}$ is much larger that T_*. This originates from the fact that large magnetically ordered clusters form already much above T_*. This fact, together with the finite polarizability of the singlet dimerized background, explains the surprisingly high Néel temperatures $T_{\rm N}$.

We can even obtain a rougher estimate of the Néel temperature. Since $T_* \ll T_{\rm N} < T_{\rm SP}$, we can, in a first approximation, take the correlation length $\xi(T)$ equal to the spin-Peierls correlation length $\xi_{\rm SP}$, and further assume that the susceptibility amounts to a paramagnetic contribution of the free magnetic moments: $\chi_{\rm s}(T) \simeq x/T$. Using equation (10) we obtain the Néel temperature

$$T_{\rm N} \simeq J_\perp x\xi_{\rm SP}, \tag{11}$$

linear in the impurity concentration. Taking $J_\perp \simeq 12$ K, and $\xi_{\rm SP} \simeq 9c$ and $x = 0.01$ we get $T_{\rm N} = 1.08$ K. At the same concentration, Martin *et al.* measure $T_{\rm N} \simeq 2$ K [6], of the same order of magnitude as our estimate.

Both equations (10, 11) are approximate expressions, which might work at intermediate impurity concentrations, but whose validity is doubtful at very low doping x. Anyhow, those results would imply that *no critical concentration is needed to get a Néel phase, since a single chain does develop quasi-long range correlations for any non zero doping*. Moreover, the Néel temperature obtained in this mean field treatment is obviously not of the order of T_*, but of the same order of magnitude than the experimental value. At this point, we judge the mean field treatment to compare satisfactory to the experimental data, given the fact that our model is certainly schematic. These results will be further confirmed by the decimation analysis in Section 4.

4 Low doping physics: decimation in 2D

We now present a decimation scheme in 2D which allows to describe the physics at extremely low doping. We have already shown in Section 3 that our model leads to correct orders of magnitude of the Néel temperature. We do not believe this mean field theory to be valid at very low doping, since lowering the doping should enhance inhomogeneities, and we then do not expect the physics to be captured by a homogeneous staggered field involved in the mean-field Stoner criterion (10). This is why we now consider the full disordered problem in a fixed dimerized background. We take a square lattice of size $L\times L$, representing the initial Cu sites of $CuGeO_3$, which, without doping, are paired into a spin-Peierls dimerized phase. Some of these lattice sites will be occupied by non magnetic impurities with a probability x, leaving in their vicinity unpaired spin 1/2 moments. The exchange coupling between two such spins at positions (x_1, y_1) and (x_2, y_2) is $H_{1-2} = J_{1-2}\mathbf{S}_1\cdot\mathbf{S}_2$, where we take

$$|J_{1-2}| = \Delta\exp\left(-\sqrt{\left(\frac{x_2-x_1}{\xi_x}\right)^2+\left(\frac{y_2-y_1}{\xi_y}\right)^2}\right), \tag{12}$$

Δ being the spin-Peierls gap $\Delta = 44.7$ K, and $\xi_x \simeq 9c$ and $\xi_y \simeq 0.1\,\xi_x$ the correlation lengths in the c and b directions, respectively. This model has no adjustable parameter. The exchange J_{1-2} is negative if the two sites belong

to the same sublattice, and positive otherwise, which takes into account the finite response of the singlet background to a staggered field. This defines a disordered spin model in 2D with long range interactions, in the sense that any spin has an exchange with any other, which however decays exponentially with their separation. The decimation procedure we use here is similar to the one used by Bhatt and Lee [32] in the study of phosphorus doped silicon. However, we decimate strong bonds without renormalizing the exchanges, which is just sufficient to get the order of magnitude of the ordering temperature.

By construction, our model has bonds which are never frustrated and are perfectly compatible with a long range AF order, being ferro on the same sublattice and antiferro on different sublattices. Therefore we may not get the same low temperature properties found by Bhatt and Lee [32] in their work on Si:P. The reason of the difference is that our spins are diluted into a matrix which is easily AF polarizable. A similar physics does not exist in Si:P.

4.1 Decimation in 2D

In one dimension, a RG transformation of a random AF spin chain consists in picking-up the strongest exchange of energy E, decimate the two corresponding spins, and renormalize the exchange by projecting onto the singlet states of the decimated bonds. This leads to broad renormalized exchange distributions and to asymptotically exact low-energy physics [30].

Similarly to the study on Si:P by Bhatt and Lee [32], we carry out the same procedure in 2D, with the difference that we do not define a renormalized exchange but just eliminate the strong bonds. This approximation is expected to lead to qualitatively correct results as far as the estimate of the ordering temperature is concerned. Considering the 2D disordered problem defined by the Hamiltonian (12), we decimate the bonds of strength $E < J \leq \Delta$. Assuming the initial bonds were colored in white, we color in black these strongly coupled bonds. As the energy E decreases, more and more white bonds will be turned into black, until the black bonds percolate throughout the system at an energy $E_{\rm P}$. We use $E_{\rm P}$ as an estimate of the Néel temperature $T_{\rm N}$, even though, strictly speaking, $E_{\rm P}$ is an upper bound of the Néel temperature. In practice, we use the following techniques to solve this problem numerically. (i) The decimation is carried out by quick sorting the exchanges. (ii) A linked list is built at each energy that encodes the graph of existing exchanges. (iii) A Hoshen-Kopelman relabeling algorithm [33] is used for cluster labeling. We have tested our program with standard 2D site and bond percolation, with excellent results. We now present our results, by first showing in Section 4.2 the failure to find a percolating cluster in the infinite volume limit. We next consider in Section 4.3 ordering in a finite coherence volume.

4.2 Absence of self similar ordering

In this section, we fix the impurity concentration x and look for percolation in an initial lattice of size $L \times L$, with increasing sizes L. Given the anisotropy of the problem ($\xi_x = 9 = 10\xi_y$), percolation occurs along the x direction of the strongest exchanges. It may happen that the left-most and right-most columns contain no impurity at low concentration, because of the finite probability Lx to have an impurity present in a given column. We are thus lead to consider as percolating a cluster that percolates between the left-most and right-most columns that contain at least one impurity.

In order to determine the percolation probability, we consider two (equivalent) quantities. First the existence probability E_L, *i.e.* the probability to find a percolating cluster in a system with a finite size L. We also consider the Binder cumulant $B_L = \langle S^2\rangle_L / \langle S\rangle_L^2$, with S the number of impurities in a percolating cluster. We analyze in this section the finite size scaling behavior of these two quantities. More precisely, if a true percolation transition would occur (as it is the case in the 2D bond and site percolation problem), the crossing points either of $E_L(T)$ or of $B_L(T)$ for increasing sizes would accumulate at the transition temperature. We have plotted in Figures 5 and 6 the existence probability and Binder cumulant for increasing sizes at a fixed impurity concentration $x = 3\%$. As it is visible in these figures, there is no true percolation transition in the sense that while the crossing point temperatures are higher and higher as the sizes increase, the existence probability decreases to zero. We interpret this result as the lack of true long range order in an infinite system. Therefore, we believe that AF ordering is of a Griffith type.

In fact, this finding is not unexpected. At a fixed energy T, we can interpret the diluted spins as particles with a core of area σ approximately given by

$$\sigma(T) \simeq \pi\xi_x\xi_y \ln^2\left(\frac{\Delta}{T}\right). \tag{13}$$

The core is indeed elliptic, with a ratio between the axes $a/b = \xi_x/\xi_y$. Hence, the ratio between the area occupied by these particles and the surface sample is

$$n_{\rm eff}(T) = x\sigma(T). \tag{14}$$

Ignoring the complication due to the anisotropy, and assuming that the cores are impenetrable, a percolating cluster can only appear if $T \leq T_{\rm P}$ where $n_{\rm eff}(T_{\rm P}) = n_{\rm c}$, being $n_{\rm c} = 0.59$ the site percolation threshold of a 2D square lattice. However, the core of each particle is not impenetrable. For this reason the existence probability does not approach one for increasing sizes even below $T_{\rm P}$. Indeed, the existence probability $E(T)$ for $L \to \infty$ does not tend to a step function as for standard percolation, but to a smooth curve as it is visible from the finite size study shown in Figure 5.

4.3 Low doping phase diagram

The previous analysis suggests that a true Néel long range order is not established at very low doping, where the singlet background is assumed only to provide a coupling between the impurity released spins. As we said, for larger

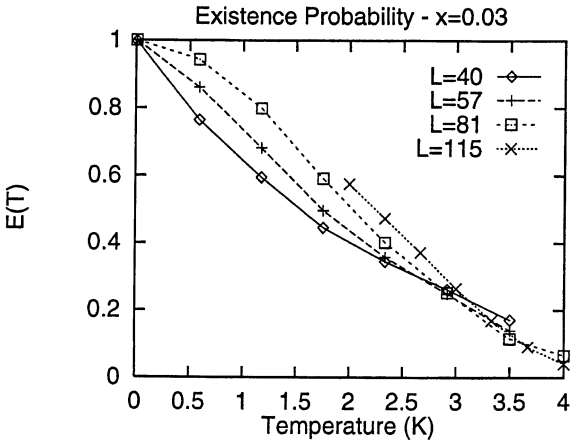

Fig. 5. Variations of the existence probability $E(T)$ *versus* temperature T at a fixed impurity concentration $x = 0.03$ and for increasing sizes $L = 40$ ($\Diamond$), $L = 57$ ($+$), $L = 81$ ($\Box$), $L = 115$ ($\times$). As it is visible in this figure, there is no self-similar fixed point.

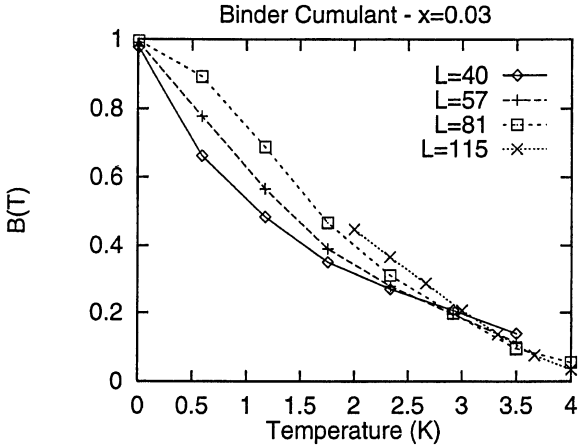

Fig. 6. Variations of the Binder cumulant $B(T)$ *versus* temperature T at a fixed impurity concentration $x = 0.03$ and for increasing sizes $L = 40$ ($\Diamond$), $L = 57$ ($+$), $L = 81$ ($\Box$), $L = 115$ ($\times$). As it is visible in this figure, there is no self-similar fixed point, in agreement with the existence probability result shown in Figure 5.

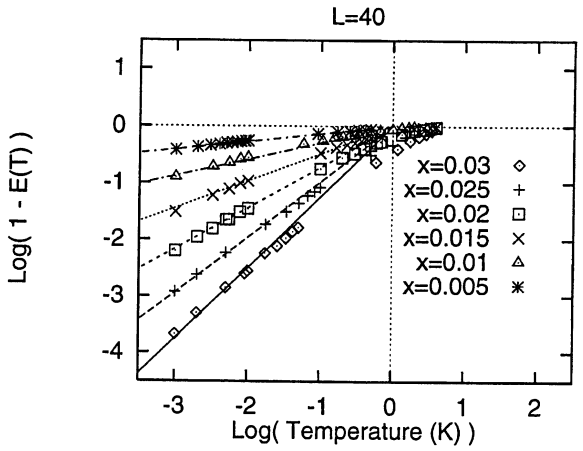

Fig. 7. Variations of $1-E(T)$ *versus* the temperature T, $E(T)$ being the existence probability for percolation of strongly coupled clusters in a system of size $L = 40$. The different curves correspond to: $x = 0.03$ and $a = 1.25$ ($\Diamond$); $x = 0.025$ and $a = 0.98$ ($+$); $x = 0.02$ and $a = 0.72$ ($\Box$); $x = 0.015$ and $a = 0.48$ ($\times$); $x = 0.01$ and $a = 0.29$ ($\triangle$); $x = 0.005$ and $a = 0.135$ ($*$). The $CuGeO_3$ parameters are $\Delta = 44.7$ K, $\xi_x = 9$ and $\xi_y = 0.1\xi_x$.

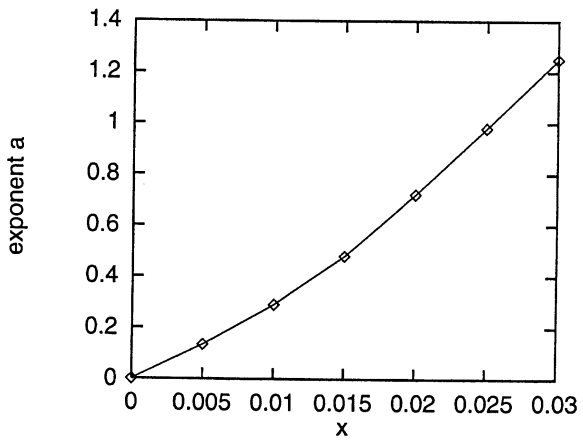

Fig. 8. Variations of the exponent a involved in the fit $1 - E(T) = T^a$ shown in Figure 7. The extrapolation to $x = 0$ and $a = 0$ has been added and is consistent with the data at higher concentrations.

doping, the background will be much more influenced by the impurities, which, besides creating states inside the gap, would also reduce the main gap, making a true antiferromagnetic long range order competitive with respect to the spin-Peierls phase, as discussed in the Introduction.

Nonetheless, the neutron beam that probes AF ordering has a finite coherence length. Therefore the relevant question, even at low doping, is not whether a true long range order exists, but rather if clusters of size larger than that coherence length appear, and with which probability. For this reason, we want now to discuss AF ordering in a finite coherence volume, which, as we said, is set either by the size of the sample or by the finite coherence length of the experimental probe, *e.g.* the neutron beam. Therefore we vary the impurity concentration x at fixed size L. The Néel temperature is estimated by imposing a fixed value of the existence probability $E_L(T) = 1/2$. We are thus forced to analyze the low temperature behavior of the existence probability $E_L(T)$. This is shown in Figure 7 for $L = 40$ and impurity concentrations between 0.5% and 3%. With these parameters, the low temperature behavior of the existence probability is well fitted by the power-law $1 - E_L(T) = T^{a(x)}$. Figure 8 shows the variations of the exponent $a(x)$ *versus* x. In this figure, we have added the point $(x = 0, a = 0)$, and, as it is visible, this extrapolation is compatible with the large x data, hence showing that zero temperature AF ordering occurs for an infinitesimal doping in a finite size. Imposing a fixed existence probability $E_L(T_N) = 1/2$, we obtain $\ln T_N \propto -1/x$, a form of the Néel temperature proposed from the low doping measurements in reference [13]. The calculated Néel

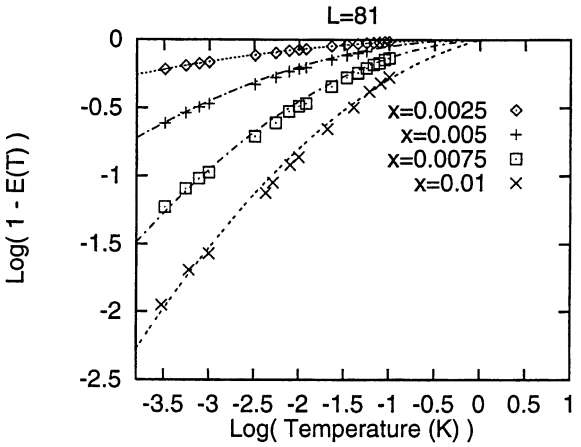

Fig. 9. Variations of $1 - E(T)$ *versus* the temperature T, $E(T)$ being the existence probability for percolation of strongly coupled clusters in a system of size $L = 81$. The fits are of the form $\log(1 - E(T)) = f(\log(T))$, with $x = 0.01$: $f(x) = -0.11x^2 + 0.18x$ ($\times$); $x = 0.0075$: $f(x) = -0.092x^2 + 0.042x$ ($\square$); $x = 0.005$: $f(x) = -0.05x^2$ ($+$); $x = 0.0025$: $f(x) = -0.018x^2$ ($\Diamond$). The $CuGeO_3$ parameters are $\Delta = 44.7$ K, $\xi_x = 9$ and $\xi_y = 0.1\xi_x$.

temperature is shown in Figure 4, together with the experimental points by Manabe *et al.* Compared to these experiments, we obtain a smaller value of the Néel temperature, still much above T_*, in agreement with [13].

In order to analyze the effect of increasing the coherence length, we now consider a system with a larger size $L = 81$. The low temperature behavior of the existence probability is shown in Figure 9, with doping concentrations from 0.25% to 1%, where the inclusion of a quadratic term was necessary in the fit. The Néel temperature obtained by imposing $E_L(T_N) = 1/2$ is shown in Figure 4, together with the $L = 40$ result and the experimental data. As it is visible in this figure, in spite of the different behavior of the low temperature existence probability $E_L(T)$ when the system size was increased from $L = 40$ to $L = 81$, the orders of magnitude of the Néel temperature $T_N(x)$ remain similar.

The above analysis suggests that at low doping the model does not have a true long range order in the thermodynamic limit, but the probability to find an ordered cluster of any given size L is finite. This implies that the system will appear as if it were ordered to an external probe with a finite coherence length. This scenario gives a natural explanation of the fact that the measured Néel temperatures are always much larger than the *typical energy scale* T_* of the doped $CuGeO_3$, and of the evidence that the intensity of the AF peaks observed in neutron scattering is not saturated even at 1.4 K [5] for a Zn doped sample with $x = 0.034$.

To obtain the dependence of the susceptibility upon temperature, we would need to improve our decimation scheme by renormalizing the exchanges, similarly to reference [32], and inserting a weak spin anisotropy, to break the spin symmetry.

Let us summarize our decimation results by comparing them to the experiments by Manabe *et al.* [13], and to T_*:

$$\text{Fit by Manabe } et\ al.\text{: } \ln T_N \sim 5.7 \times 10^{-3}/x \quad (15)$$

$$\text{Decimation } (L = 40, 81)\text{: } \ln T_N \sim 10^{-3}/x \quad (16)$$

$$\text{Behavior of } T_*\text{: } \ln T_* \sim 10^{-1}/x, \quad (17)$$

which illustrates both the fact that we can reproduce sucessfully the absence of critical concentration in our model, and the crucial role of disorder in enhancing the Néel temperature.

5 Conclusion and discussion

Let us summarize the proposal we have presented for the onset of the Néel long range order in doped $CuGeO_3$. We first want to stress that, in our opinion, the real difficulty in the subject is not the coexistence of dimerization and antiferromagnetism, since the two order parameters are not incompatible. Instead, what is puzzling is the appearance of antiferromagnetism at such low impurity concentration as 1×10^{-3}, with a reasonably high transition temperature. We have shown that this behavior might depend on the peculiar properties of the disorder in this system, as well as in other spin gaped systems.

We believe that the most important effect of disorder, at low doping, is to induce randomly distributed localized free moments. These moments are weakly coupled by an exchange constant exponentially decaying upon the distance, see equation (3), caused by the virtual polarization of the singlet background. We have shown that even a single chain does develop quasi long range Néel order, *i.e.* a power law decaying staggered correlation function, which, we believe, does imply a low temperature transition to an AF phase as soon as the interchain exchange is taken into account. Moreover, we argued that the exponential dependence on the distance of the exchange between those randomly distributed moments implies that rare events in which the impurity released spins are closer than the average distance (and therefore get strongly coupled), dominate the physics at low doping, in a Griffith-like scenario. This picture was fully confirmed by an investigation of the 2D disordered problem using a decimation method. The formation of these Griffith-like clusters, together with the finite staggered susceptibility of the singlet background, may explain why ordered domains larger that the neutron coherence length do appear at temperatures much larger than the temperature T_* (the exchange between two moments at a distance equal to the average one).

Some consequences can be drawn from this scenario:

- A Néel transition is expected for any arbitrary small impurity concentration.
- At relatively large doping concentrations, the mean field picture is expected to hold since the inhomogeneities of the AF order are weak. In this concentration range, the Néel temperature behaves like $T_N \simeq J_b \xi_{SP} x$, where J_b is the exchange constant in the b-direction, and ξ_{SP} the correlation length in the pure $CuGeO_3$.

– For low impurity concentrations, the Néel state becomes highly inhomogeneous and the decimation method is more suited than the mean field theory. Instead of a single transition temperature we find a quite broad distribution of T_N's. We have indications that a true long range order is never established, so that the low temperature phase might be rather interpreted as a Griffith-like antiferromagnet. We have shown that, for small coherence volumes, the Néel temperature behaves like $\ln T_N \sim -1/x$. By increasing the coherence volume, this behavior does not rigorously hold. However, as it is visible in Figure 4, the behavior of the Néel temperature for $L = 81$ can hardly be discriminated from the $L = 40$ calculation, and a fit of our results to a $\ln T_N \sim -1/x$ behavior would be equally satisfactory.
– A very long correlation length in the c-axis direction, extending well above ξ_{SP}, may be observed in a wide temperature range. This can be measured in NMR experiments at very low doping. For instance, the NMR linewidth in the ladder compound $Sr(Cu_{1-x}Zn_x)_2O_3$ at a Zn concentration $x = 0.25\%$, at which no Néel transition has been observed down to the lowest accessible temperature, is two orders of magnitude larger than the correlation length of the undoped compound [34], which indicates that a similar behavior might well occur in the doped $CuGeO_3$.

We now compare our results with other theoretical proposals. We first compare our work to the one by Mostovoy *et al.* [15], and next to the work by Fukuyama *et al.* [14], and Yoshioka and Suzumura [19]. The technicalities involved in the discussion of these last two works are left in the Appendices A and B, and we focus here in the concluding section on more qualitative aspects.

Mostovoy *et al.* [15] have recently investigated the effects of interchain coupling at a mean field level in an antiferromagnetic Heisenberg chain with random dimerization, modeled by a δ-correlated in space Gaussian-distribution peaked around a finite average value. In order to make contact with their work, we make the following comments:

(i) The microscopic modeling of doping in a spin-Peierls system is quite different in our model and in reference [15]. As we showed in reference [16], our model is more related to a dimerization with a random telegraph noise of zero average distribution, with the low temperature physics dominated by the localized spins around the domain walls.
(ii) The physics of the 1D limit of both models is different. This can be seen by considering the RG flow [29,30]. The 1D limit of the model by Mostovoy *et al.* has been solved by Hyman *et al.* [35], and flows to a fixed point with power-law Griffith singularities. By contrast, the 1D limit of our model flows to the random singlet fixed point [30] with logarithmic singularities [16,17].
(iii) More importantly, the random dimerized Heisenberg chain, which is the starting point of the description in reference [15], does *not* develop quasi long range AF fluctuations, as it is the case in our proposal. This allows to understand why a finite critical concentration of impurities is required in reference [15] to generate an AF-dimerized phase. As we show in the present article, this is not the case in our model, and it seems that this is not the case in experiments either [13].

A proposal similar to the one by Mostovoy *et al.* was previously put forward by Fukuyama, Tanimoto and Saito (FTS) [14], who also worked out a model showing a coexistence of antiferromagnetism and dimerization, as well as the onset of antiferromagnetism for arbitrary small doping. As we discussed, we have started our analysis by assuming that the main effect of the impurities is the release of free spins out of the singlet background, which is in agreement with the magnetic susceptibility data on the doped compounds, showing an almost Curie like component at low temperature which seems to scale linearly with doping (see for instance Refs. [9,13]). Instead, FTS assume, as Mostovoy *et al.*, that the main effect of disorder is the local reduction of the dimerization $\delta_{imp} < \delta$ close to each impurity, hence of the spin gap. For instance, they can fit the experimental reduction of the scattering intensity from the dimerized lattice in the 0.7% Si doped compound, by taking $\delta_{imp} \sim 0.2\delta$. This leads to a rough estimate of the local reduction of the spin gap $\Delta_{imp} \sim (0.2)^{2/3}\Delta \simeq 0.9\Delta$. Obviously, for smaller impurity concentrations, one should expect an even smaller reduction of the spin gap. However, to explain within this model the almost Curie like behavior of the low temperature susceptibility at low doping, one should assume a much stronger suppression of the spin gap down to ~ 10 mK close to each impurity, not just a small reduction as the fit to the neutron scattering data would imply. This is one reason why we believe that our approach is more relevant. The other is that we do not believe that a local reduction of the dimerization might explain the appearance of antiferromagnetism at such low concentration as 0.1% of Zn doping.

In fact, a more realistic modeling of disorder in $CuGeO_3$ should include both disorder effects, the local reduction of dimerization as well as the appearance of free spins. Essentially, the main difference between our approach and the FTS one is in the different emphasis placed on the two effects. We believe that the main role at low doping in establishing the Néel phase is played by the free moments induced by disorder, while FTS seem to favor the other mechanism of a local reduction of the dimerization.

Apart from this comment on the grounds of the model proposed in reference [14], we also have some more technical criticisms. To analyze their model, FTS use the so-called Self Consistent Harmonic Approximation (SCHA) applied to the bosonized version of a dimerized Heisenberg chain. This approximation is a mean field theory, or saddle point approximation, plus random phase fluctuations. By this technique, they show the existence of a mean field solution having both a finite dimerization parameter and a finite Néel order parameter. Essentially, close to the impurity, where the dimerization parameter is assumed to be

reduced, a staggered magnetic moment in the z-direction arises. We believe that this approach is not fully consistent, as we explain in detail in Appendix A.

An alternative variational approach has recently been developed by Yoshioka and Suzumura [19] for the Zn doping case. They have rigorously shown that in bosonization the spin-lattice coupling does change sign crossing a non magnetic impurity, as it was proposed in reference [16]. With this disorder modeling they have proved the existence of a variational action which does again describe a state where the dimerization gets reduced around an impurity and at the same time a static staggered moment appears in the z-direction. We believe that this variational approach gives a reasonable description of the Néel ordered phase, very close to what we propose, but does not allow a description of how the AF ordering occurs, which we did in the present work. We postpone to Appendix B a detailed discussion of this point, and we end-up with two simple comments on these semiclassical analyzes.

The dimerized phase breaks translational invariance like a Néel phase does, which, in addition, also breaks spin symmetry. If one analyzes the role of defects in a dimerized state within a scheme which breaks SU(2) symmetry (what is implicitly done in those semiclassical approaches, as shown in Appendix B), it is not a surprise that a finite staggered magnetization comes out of the calculation (without spin anisotropy or an applied staggered magnetic field), since the dimerized state already breaks translational symmetry.

Finally, one can work out a model in the spirit of the FTS scenario. This can be done by considering a dimerization distributed as a telegraph noise, and taking a value δ in the dimerized background (large segments), and $0 < \delta_{\rm imp} < \delta$ close to the impurities (short segments). The resulting disordered model can be exactly solved in the XX limit along the lines in reference [36]. This would result in a model with power-law Griffith singularities, equivalent to the model by Mostovoy *et al.* [15], and inequivalent to our model where the Dyson singularities are logarithmic. This model would not flow to the random singlet fixed point [30], would have much weaker AF fluctuations than our model, and, as in the case of the model by Mostovoy *et al.*, a critical concentration would be expected for the appearance of AF order.

We acknowledge useful discussions with J.C. Anglès d'Auriac, C. Berthier, D. Fisher, T. Giamarchi, B. Grenier, M. Horvatic, J.C. Lasjaunias, J. Lorenzo, P. Monceau, A. Nersesyan, Y. Okabe, C. Paulsen, J.P. Pouget, G. Remenyi and M. Saint-Paul at various stages of this project. The authors also thank K. Uchinokura for sending them their susceptibility data. This work has been partly supported by INFM, Research Project HTSC. The decimation calculations have been performed on the CRAY T3E supercomputer of the Centre de Calcul Vectoriel Grenoblois of the Commissariat à l'Énergie Atomique.

Appendix A: Self consistent harmonic approximation

In this Appendix, we discuss the Self Consistent Harmonic Approximation (SCHA) approach used by Fukuyama, Tanimoto and Saito (FTS) in reference [14]. We do not want to enter in the details of the transformation which allows to map the spin-Peierls problem onto a bosonic one, since they can be found in reference [14], and references therein. We assume that this transformation is valid, and, following [14], that the resulting bosonic Hamiltonian is

$$\hat{H} = \frac{1}{2}\int \mathrm{d}x \big[\Pi(x)^2 + (\partial\phi(x))^2 - 2gu(x)\sin\left(\sqrt{4\pi K}\phi(x)\right) + \kappa u^2(x)\Big], \quad \text{(A.1)}$$

where $\phi(x)$ and $\Pi(x)$ are bosonic conjugate fields. The classical variable $u(x)$ represents the dimerization lattice distortion, and the $\sin(\dots)$ is the spin dimerization order parameter. Notice that the $\cos(\dots)$ would represent the z-component of the staggered magnetization. We then write $\phi(x) = \phi_{\rm c}(x) + \phi(x)$, where $\phi_{\rm c}(x)$ is a classical variable, and $\phi(x)$ is the quantum fluctuation part, which is assumed to have a zero average value. We want to find the minimum of the total energy assuming a bosonic state $|0\rangle$ which is the ground state of the following Hamiltonian

$$\hat{H}_{\rm sc} = \frac{1}{2}\int \mathrm{d}x \left[\Pi(x)^2 + (\partial\phi(x))^2 + m(x)\phi^2(x)\right], \quad \text{(A.2)}$$

with $m(x) > 0$. Therefore we have to find the appropriate values of $\phi_{\rm c}(x)$, $u(x)$ and $m(x)$ which minimize the average value of $\hat{H}$ over $|0\rangle$. This is the so-called Self Consistent Harmonic Approximation (SCHA), which is a well defined variational technique. Since (A.2) is quadratic, then $\langle 0|\phi(x)|0\rangle = 0$, and

$$\langle 0|\sin\left(\sqrt{4\pi K}\left(\phi_{\rm c}(x)+\phi(x)\right)\right)|0\rangle = D(x)\sin\left(\sqrt{4\pi K}\phi_{\rm c}(x)\right),$$

where $D(x) = \mathrm{e}^{-2\pi K\langle\phi(x)^2\rangle}$. If we define $T(x) \equiv \langle \Pi^2(x) + (\partial\phi(x))^2\rangle$, the self-consistent equations are

$$-\partial^2\phi_{\rm c}(x) - g\sqrt{4\pi K}u(x)D(x)\cos\left(\sqrt{4\pi K}\phi_{\rm c}(x)\right) = 0; \quad \text{(A.3)}$$

$$\kappa u(x) = gD(x)\sin\left(\sqrt{4\pi K}\phi_{\rm c}(x)\right); \quad \text{(A.4)}$$

$$\int \mathrm{d}y \frac{\delta T(y)}{\delta m(x)} + 4\pi K g u(y)\sin\left(\sqrt{4\pi K}\phi_{\rm c}(y)\right)D(y)\frac{\delta\langle\phi(y)^2\rangle}{\delta m(x)} = 0, \quad \text{(A.5)}$$

where we used

$$\frac{\delta D(y)}{\delta m(x)} = -2\pi K D(y)\frac{\delta\langle\phi(y)^2\rangle}{\delta m(x)}\,.$$

We start by solving (A.5). We write the bosonic fields as

$$\phi(x) = \sum_\alpha \frac{1}{\sqrt{2\epsilon_\alpha}} \varphi_\alpha(x) \left(b_\alpha + b^\dagger_{-\alpha} \right), \tag{A.6}$$

$$\Pi(x) = i \sum_\alpha \sqrt{\frac{\epsilon_\alpha}{2}} \varphi^*_\alpha(x) \left(b^\dagger_\alpha - b_{-\alpha} \right), \tag{A.7}$$

where $\varphi_{-\alpha}(x) = \varphi^*_\alpha(x)$, $\epsilon_\alpha = \epsilon_{-\alpha}$,

$$\sum_\alpha \varphi^*_\alpha(x)\varphi_\alpha(y) = \delta(x-y),$$

and $[b_\alpha, b^\dagger_\beta] = \delta_{\alpha,\beta}$, all other commutators being zero. We want the Hamiltonian (A.2) to be diagonal in terms of these creation and annihilation operators:

$$\hat{H}_{\rm sc} = \sum_\alpha \epsilon_\alpha b^\dagger_\alpha b_\alpha.$$

A straightforward calculation gives

$$-\partial^2 \varphi_\alpha(x) + m(x)\varphi_\alpha(x) = \epsilon^2_\alpha \varphi_\alpha(x), \tag{A.8}$$

which is the eigenvalue equation for φ_α. On the bosonic vacuum of the operators b_α, we find that

$$\int {\rm d}y\, T(y) = \frac{1}{2} \sum_\alpha \int {\rm d}y \Big[\epsilon_\alpha\, \varphi^*_\alpha(y)\varphi_\alpha(y) + \frac{1}{\epsilon_\alpha} \partial\varphi^*_\alpha(y) \partial\varphi_\alpha(y) \Big],$$

which, through equation (A.8), becomes

$$\begin{aligned} \int {\rm d}y T(y) &= \sum_\alpha \frac{1}{2\epsilon_\alpha} \int {\rm d}y \left(2\epsilon^2_\alpha - m(y) \right) \varphi^*_\alpha(y)\varphi_\alpha(y) \\ &= \sum_\alpha \left[\epsilon_\alpha - \int {\rm d}y \frac{m(y)}{2\epsilon_\alpha} \varphi^*_\alpha(y)\varphi_\alpha(y) \right] \\ &= \sum_\alpha \epsilon_\alpha - \int {\rm d}y\; m(y) \langle \phi^2(y) \rangle, \end{aligned}$$

where the last identity follows from (A.6). Now, suppose that $m(x) \to m(x) + \delta m(x)$. It is easy to get the first order correction to the eigenvalues through (A.8):

$$\begin{aligned} \sum_\alpha \delta\epsilon_\alpha &= \sum_\alpha \frac{1}{2\epsilon_\alpha} \int {\rm d}y\, \varphi^*_\alpha(y)\, \delta m(y)\, \varphi_\alpha(y) \\ &= \int {\rm d}y\, \delta m(y) \langle \phi^2(y) \rangle. \end{aligned}$$

Through the above equations we find that

$$\int {\rm d}y\, \frac{\delta T(y)}{\delta m(x)} = \langle \phi^2(x) \rangle - \left[\langle \phi^2(x) \rangle + \int {\rm d}y\, m(y) \frac{\delta \langle \phi^2(y) \rangle}{\delta m(x)} \right],$$

which, inserted in equation (A.5) gives

$$\int {\rm d}y \left[-m(y) + 4\pi K g u(y) \sin\left(\sqrt{4\pi K}\phi_{\rm c}(y) \right) D(y) \right] \times \frac{\delta \langle \phi^2(y) \rangle}{\delta m(x)} = 0.$$

This equation is solved by imposing

$$m(x) = 4\pi K g u(x) \sin\left(\sqrt{4\pi K}\phi_{\rm c}(x) \right) {\rm e}^{-2\pi K \langle \phi(x)^2 \rangle}, \tag{A.9}$$

which gives the self-consistent equation for the mass.

As a simple application, let us consider the homogeneous case $m(x) = m$, $u(x) = u$, and $\phi_{\rm c}(x) = \phi_{\rm c}$ for any x. From equation (A.3) we get

$$\sqrt{4\pi K}\phi_{\rm c}(x) = \pi(n + \frac{1}{2}), \tag{A.10}$$

which choice is in fact the only compatible with SU(2) symmetry. We choose $n = 1$. On the other hand equation (A.8) is solved by plane waves

$$\varphi_q(x) = \frac{1}{\sqrt{L}} {\rm e}^{-{\rm i}qx},$$

with energy $\epsilon_q = \sqrt{q^2 + m}$. Therefore

$$\langle \phi(x)^2 \rangle = \frac{1}{2L} \sum_q \frac{1}{\sqrt{q^2+m}} \simeq \frac{1}{4\pi} \log\left(\frac{m_0}{m} \right),$$

where m_0 is a high-energy cut-off, and (A.9) becomes

$$m = 4\pi K g u \left(\frac{m}{m_0} \right)^{K/2}.$$

The solution is $m \sim (gu)^{2/(2-K)}$. Since the approach is valid only if, for a small coupling g, a small mass m is obtained, the above equation implies that a mass is generated if $K < 2$. This is the famous result for the sine-Gordon models. If we consider this model as describing a spin-Peierls transition, we know that $K = 1$ corresponds to the XX-limit and $K = 1/2$ to the SU(2) point. In the latter case,

$$m = 2\pi g u \left(\frac{m}{m_0} \right)^{1/4}.$$

Equation (A.4) is solved by

$$u = \frac{g}{\kappa} \left(\frac{m}{m_0} \right)^{1/4},$$

finally leading to

$$m = \frac{4\pi^2 g^4}{\kappa^2 m_0}. \tag{A.11}$$

Now let us consider the inhomogeneous case. For instance, following FTS [14], we assume that $u(0) = u(l) = u_i$. Through (A.9) the self consistent equations can be written as

$$-\partial^2\phi_{\rm c}(x) - g\sqrt{4\pi K}u(x)D(x)\cos\left(\sqrt{4\pi K}\phi_{\rm c}(x)\right) = 0; \tag{A.12}$$

$$\kappa u(x) = gD(x)\sin\left(\sqrt{4\pi K}\phi_{\rm c}(x)\right); \tag{A.13}$$

$$m(x) = 4\pi K g u(x)\sin\left(\sqrt{4\pi K}\phi_{\rm c}(x)\right)D(x). \tag{A.14}$$

Solving for $u(x)$, we get

$$u^2(x) = \frac{1}{4\pi K\kappa}m(x),$$

and the coupled equations for $m(x)$ and $\phi_{\rm c}(x)$ read

$$m(x) = \frac{4\pi K g^2}{\kappa}D^2(x)\sin^2\left(\sqrt{4\pi K}\phi_{\rm c}(x)\right), \tag{A.15}$$

$$-\partial^2\phi_{\rm c}(x) - \frac{g^2\sqrt{4\pi K}D^2(x)}{2\kappa}\sin\left(2\sqrt{4\pi K}\phi_{\rm c}(x)\right) = 0. \tag{A.16}$$

We do not know whether these equations have a unique solution. FTS implicitly assume that $D(x)$ as well as $m(x)$ are independent of x. Then equation (A.13) at $x = 0, l$ fixes the value of $\phi_{\rm c}(0)$ and $\phi_{\rm c}(l)$, which are used as boundary conditions to solve equation (A.16). The solution is a Jacobi elliptic function. Between $x = 0$ and $x = l$, the solution approaches the homogeneous one (A.10), but around these points it is different. As a result, $\sin^2\left(2\sqrt{4\pi K}\phi_{\rm c}(x)\right)$ differs from one close to $x = 0$ and $x = l$, leading to a finite value of $\cos^2\left(2\sqrt{4\pi K}\phi_{\rm c}(x)\right)$, hence to a finite staggered magnetization. This result would imply that disorder in the lattice distortion leads automatically to a long range Néel phase, but necessarily with a staggered magnetization along z. In fact, the staggered magnetization perpendicular to z is expressed in terms of the conjugate momentum $\Pi(x)$, which is uncertain if $\phi_{\rm c}(x)$ gets an average value. This result is puzzling, since the starting Hamiltonian is spin isotropic. Moreover, the assumptions $D(x)$ and $m(x)$ x-independent have to be *a posteriori* verified. FTS do not make this check, but clearly, by inspection of equation (A.15), one realizes that the assumption is not correct. Therefore the calculations of reference [14] are not self-consistent.

Alternatively, one can look for a solution which does not break SU(2) symmetry. In this case we have to assume a constant $\phi_{\rm c}(x) = \pi/2$, compatible with (A.10). Therefore one needs to solve

$$\kappa u(x) = gD(x); \tag{A.17}$$

$$m(x) = 2\pi g u(x)D(x), \tag{A.18}$$

or, equivalently,

$$m(x) = \frac{2\pi}{\kappa}g^2D^2(x) = 2\pi\kappa u^2(x),$$

with the boundary conditions $m(0) = m(l) = 2\pi\kappa u_i^2$. If this equation were solvable, we would get an alternative solution which keeps the SU(2) symmetry. Further work to establish which is the best self-consistent solution is needed, but we can safely state that the assumption of homogeneous quantum fluctuations made in reference [14] is not self-consistent.

Appendix B: Some rigorous results in the presence of solitons

In order to better clarify the limits of the SCHA, we consider a simple case which is related to the work by Yoshioka and Suzumura [19]. These authors have proved by bosonization that the coupling to the lattice changes sign crossing a non magnetic ions. A similar conclusion was reached in reference [16], by means of a simple mapping to a squeezed chain where the non magnetic sites are eliminated. This mapping is explained in Figure 1. The squeezed chain is obtained by eliminating the non magnetic site similarly to what is done in the $U \to \infty$ Hubbard model. The difference here is that the *hole* does not move. Next, the weak link across the impurity is approximated as the weak bond of the dimerized pattern, *i.e.* $J(1-\delta)$, which is supposed not to change qualitatively the low energy physics. Hence, the effective model describing the squeezed chain consists of a dimerized Heisenberg chain with a domain wall. The model in the presence of a single domain wall can also be analyzed along the same lines outlined in reference [19]. The result would be again that a variational solution can be obtained with a space dependent classical phase $\phi_{\rm c}(x)$, but a space independent mass for the bosons describing the quantum fluctuations. The same would hold also in the XX-limit, which can be also easily solved by diagonalizing the spinless fermion Hamiltonian which is obtained through a Jordan-Wigner transformation. In the continuum limit and after linearizing the band around the Fermi momenta $k_{\rm F} = \pm\pi/2$, one has to solve the following equations

$$-{\rm i}\frac{\partial}{\partial x}\chi_{\epsilon{\rm R}}(x) - {\rm i}\Delta(x)\chi_{\epsilon{\rm L}}(x) = \epsilon\chi_{\epsilon{\rm R}}(x), \tag{B.1}$$

$${\rm i}\frac{\partial}{\partial x}\chi_{\epsilon{\rm L}}(x) + {\rm i}\Delta(x)\chi_{\epsilon{\rm R}}(x) = \epsilon\chi_{\epsilon{\rm L}}(x), \tag{B.2}$$

where the Fermi field is expressed in terms of the χ functions through

$$\begin{aligned}\Psi(x) &= \sum_\epsilon \left[{\rm e}^{{\rm i}k_{\rm F}x}\chi_{\epsilon{\rm R}}(x) + {\rm e}^{-{\rm i}k_{\rm F}x}\chi_{\epsilon{\rm L}}(x)\right]c_\epsilon \\ &\equiv \sum_\epsilon \phi_\epsilon(x)c_\epsilon,\end{aligned}$$

c_ϵ being the annihilation operator of an eigenstate of energy ϵ. The dimerization parameter is equal to Δ for $x < 0$, and to $-\Delta$ at $x > 0$, thus having a domain wall at $x = 0$. equations (B.1, B.2) can be solved and one finds, in addition to scattering solutions with energy $\epsilon = \pm\sqrt{k^2 + \Delta^2}$,

k being the wavevector, a localized zero energy solution with wavefunction

$$\phi_0(x) = \sqrt{2\Delta}\mathrm{e}^{-|x|\Delta}\sin(k_\mathrm{F}x).$$

This is a soliton solution for a single domain wall.

The classical phase which appears in the bosonized version of the model can be related to the phase of the $2k_\mathrm{F}$ oscillating part of the spinless fermion density. Namely, we expect that

$$\rho_{2k_\mathrm{F}}(x) = \langle\Psi^\dagger(x)\Psi(x)\rangle_{2k_\mathrm{F}} \sim \cos\left(2k_\mathrm{F}x + \phi_\mathrm{c}(x)\right). \quad \text{(B.3)}$$

The dimer order corresponds to a bond ordered Charge Density Wave (CDW), *i.e.* $\phi_\mathrm{c}(x) = (2n+1)\pi/2$, while the Néel phase to a site ordered CDW, *i.e.* $\phi_\mathrm{c}(x) = n\pi$. In the absence of the domain wall, the phase is $\phi_\mathrm{c}(x) = (2n+1)\pi/2$ at any x. In addition, in the presence of the domain wall, two other terms arise. One is

$$\rho_1(x) = \left(n_0 - \frac{1}{2}\right)\Delta\mathrm{e}^{-2|x|\Delta}\left(1 - \cos(2k_\mathrm{F}x)\right), \quad \text{(B.4)}$$

where n_0 is the occupation probability of the soliton state. In fact, the term proportional to n_0 is the soliton wave function density probability, while the other one comes from the negative energy scattering solutions. We notice that ρ_1 oscillates with a phase which has two possible values $\phi_\mathrm{c} = 0, \pi$ depending on n_0, which are compatible with the two possible Néel ordered phases. The other term which is generated by the domain wall decays like

$$\rho_2(x) \sim \frac{\sin(2k_\mathrm{F}x)}{\sqrt{\Delta x}}\mathrm{e}^{-2|x|\Delta}, \quad \text{(B.5)}$$

and generates the polarization of the background responsible for the coupling among consecutive solitons, which we have considered throughout this work. This term oscillates with a phase compatible with a dimer order. Were $\rho_1(x)$ be present, we would indeed find a coexistence of dimer order and Néel one, the latter mainly localized close to the domain wall.

We have now all the elements to describe what happens in this solvable model for the classical phase, and compare with the variational approach of reference [19]. We start reminding that after the Jordan-Wigner transformation, a site occupied by a spinless fermion corresponds to a the spin having a z-component $S_z = 1/2$, while an empty site to $S_z = -1/2$. Moreover, a chain with periodic boundary conditions is compatible with the presence of a single domain wall only if it has an odd number of sites. Therefore the ground state has a total $S = 1/2$. In our XX-limit we can not rigorously discuss the SU(2) symmetry, but at least the following discussion gives some hints how the implementation of such symmetry gives a classical phase $\phi_\mathrm{c}(x) = \pi/2$ independent of the position. In fact, if we take a ground state which does not break the symmetry, we have to assume that the chemical potential crosses exactly the soliton energy, so that there is an equal probability to have $S_z = \pm 1/2$. In other words this implies that $n_0 = 1/2$, leading to a vanishing $\rho_1(x)$, and leaving only the $\rho_2(x)$ term which has indeed a phase fixed at $\phi_\mathrm{c}(x) = \pi/2$. Let us suppose a domain wall and an anti-domain wall at a distance much larger that $1/\Delta$. We can now consider a periodic chain with an even number of sites. The ground state will be a singlet. Around each domain wall there will be a localized soliton state at zero energy. The two $S = 1/2$ solitons will be coupled by the polarization of the background, generating a singlet $S = 0$ as well as a triplet $S = 1$ state. The singlet state has energy $-t$ ($0 < t \ll \Delta$), the $S_z = 0$ component of the triplet $+t$, and the $S_z = \pm 1$ have energy zero, where t decays exponentially with the distance among the two domain walls. The fact that the triplet is not degenerate is a consequence of the XX-limit. In this case, however, we are lucky since the lowest energy state, being a singlet, is SU(2) invariant. This is in essence why the spin anisotropy with a random distribution of domain walls does not play a very relevant role for what it regards the ground state properties. Within the lowest energy singlet state, each soliton state has an equal probability of being empty or occupied, leading again to a vanishing $\rho_1(x)$ equation (B.4). However, one can view the singlet state as oscillating between two configurations each having $\rho_1(x) \neq 0$, hence a classical phase $\phi_\mathrm{c} = 0, \pi$ compatible with a Néel order. In a rough picture, the system is locally, in time, in one of the two possible Néel ordered states, and oscillates between them over a very long time scale $\sim 1/t$. Moreover, in spite of the exponential decay of the polarization over a length $\xi_\mathrm{SP} \sim 1/(2\Delta)$, which is the correlation length of the dimerized state, the two solitons, which are at a distance much larger that ξ_SP, oscillate coherently. This is on a very small scale our picture of what happens in the doped $CuGeO_3$.

We think that the variational approach of reference [19] is able to describe only the states where one soliton is occupied and the other is empty, or *vice versa*, and not the superposition of the two, which is beyond a mean field like approach. Therefore the method implicitly breaks SU(2) symmetry, which obviously leads to a finite staggered magnetization $\rho_1(x)$, since already the dimerized state breaks the translational invariance. For this reason, we believe that this approach should give a reasonable description of the Néel ordered phase, but is unable to describe the way in which the magnetic ordering is established, which is what we have done in this work.

References

1. M. Hase, I. Terasaki, K. Uchinokura, Phys. Rev. Lett. **70**, 3651 (1993); J.P. Pouget, L.P. Regnault, M. Ain, B. Hennion, J.P. Renard, P. Veillet, G. Dhalenne, A. Revcolevschi, Phys. Rev. Lett. **72**, 4037 (1994).
2. J.-G. Lussier, S.M. Coad, D.F. McMorrow, D. McK Paul, J. Phys. Cond. Matter **7**, L325 (1995).
3. P.E. Anderson, J.Z. Liu, R.N. Shelton, Phys. Rev. B **56** (1997), 11014.
4. M. Hase, N. Koide, K. Manabe, Y. Sasago, K. Uchinokura, A. Sawa, Physica B **215**, 164 (1995).
5. M. Hase, K. Uchinokura, R.J. Birgeneau, K. Hirota, G. Shirane, J. Phys. Soc. Jap. **65**, 1392 (1996).

6. M.C. Martin, M. Hase, K. Hirota, G. Shirane, Phys. Rev. B **56**, 3173 (1997).
7. T. Masuda, A. Fujioka, Y. Uchiyama, I. Tsukada, K. Uchinokura, Phys. Rev. Lett. **80**, 4566 (1998).
8. J.-P. Renard, K. Le Dang, P. Veillet, G. Dhalenne, A. Revcolevschi, L.P. Regnault, Europhys. Lett. **30**, 475 (1995); L.P. Regnault, J.P. Renard, G. Dhalenne, A. Revcolevschi, Europhys. Lett. **32**, 579 (1995).
9. B. Grenier, J.P. Renard, P. Veillet, C. Paulsen, R. Calemcsuk, G. Dhalenne, A. Revcolevschi, Phys. Rev. B **57** (1998), 3444.
10. M. Saint-Paul, J. Voiron, C. Paulsen, P. Monceau, G. Dhalenne, A. Revcolevschi, J. Phys. Cond. Matter **10**, 10215 (1998).
11. Isolated Co^2+ is in a spin 3/2 orbitally degenerate multiplet. Due to the orbital degeneracy, which is unclear if and how is split in $CuGeO_3$, it is still not possible to construct a realistic model for describing Co doping.
12. B. Grenier, J.P. Renard, P. Veillet, L.P. Regnault, J.E. Lorenzo, C. Paulsen, G. Dhalenne, A. Revcolevschi, *Universal phase diagram of Si-, Zn-, Mg- and Ni-doped $CuGeO_3$: spin-Peierls order and antiferromagnetism*, preprint (1998).
13. K. Manabe, H. Ishimoto, N. Koide, Y. Sasago, K. Uchinokura, Phys. Rev. B **58**, R575 (1998).
14. H. Fukuyama, T. Tanimoto, M. Saito, J. Phys. Soc. Jap. **65**, 1182, 1996.
15. M. Mostovoy, D. Khomskii, J. Knoester, Report No cond-mat/9712098.
16. M. Fabrizio, R. Mélin, Phys. Rev. Lett. **78**, 3382 (1997).
17. M. Fabrizio, R. Mélin, Phys. Rev. B **56**, 5996 (1997).
18. M. Azuma, Y. Fujishiro, M. Takano, M. Nohara, H. Takagi, Phys. Rev. B **55**, R8658 (1997); M. Azuma, M. Takano, R.S. Eccleston, J. Phys. Soc. Jap. **67**, 740 (1998); N. Fujiwara, H. Yasuoka, Y. Fujishiro, M. Azuma, M. Takano, Phys. Rev. Lett. **80**, 604 (1998).
19. H. Yoshioka, Y. Suzumura, J. Phys. Soc. Jap. **66**, 3962 (1997).
20. L.P. Regnault, A. Aïn, B. Hennion, G. Dhalenne, A. Revcolevschii, Phys. Rev. B **53**, 5579 (1996).
21. J. Riera, A. Dobry, Phys. Rev. B **51**, 16098 (1995); C. Castilla, S. Chakravarty, V.J. Emery, Phys. Rev. Lett. **75**, 1823 (1995).
22. G.B. Martins, E. Dagotto, J.A. Riera, Phys. Rev. B **54**, 16032 (1996).
23. M. Laukamp, G.B. Martins, C. Gazza, A.L. Malvezzi, E. Dagotto, P.M. Hansen, A.C. López, J. Riera, Phys. Rev. B **57**, 10755 (1998).
24. P.M. Hansen, J.A. Riera, A. Delia, E. Dagotto, Phys. Rev. B **58**, in press (1998).
25. P. Hansen, D. Augier, J. Riera, D. Poilblanc, Report No cond-mat/9805325.
26. D. Augier, P. Hansen, D. Poilblanc, J. Riera, E. Sorensen, Report No cond-mat/9805386.
27. M. Braden, G. Wilkendorf, J. Lorenzana, M. Aïn, G.J. McIntyre, M. Behruzi, G. Heger, G. Dhalenne, A. Revcolevschi, Phys. Rev. B **54**, 1105 (1996).
28. Kiryukin *et al.* have measured a soliton half-width $\xi_{SP} = 13.6c$ (V. Kiryukin, B. Keimer, J.P. Hill, A. Vigliante, Phys. Rev. Lett. **76**, 4608 (1996)). However, recent NMR experiments (M. Horvatic *et al.*, preprint) have measured a smaller soliton width, of the order of $\xi_{SP} \sim 9c$.
29. C. Dasgupta, S.K. Ma, Phys. Rev. B **22**, 1305 (1980).
30. D. Fisher, Phys. Rev. B **50**, 3799 (1994).
31. This is the typical behavior of a random Heisenberg chain as obtained by D. Fisher in reference [30].
32. R.N. Bhatt, P.A. Lee, Phys. Rev. Lett. **48**, 344 (1982).
33. J. Hoshen, R. Kopelman, Phys. Rev. B **14**,3438 (1976).
34. N. Fujiwara, H. Yasuoka, Y. Fujishiro, M. Azuma, M. Takano, Phys. Rev. Lett. **80**, 604 (1998).
35. R.A. Hyman, K. Yang, R.N. Bhatt, S.M. Girvin, Phys. Rev. Lett. **76**, 839 (1996).
36. A. Comtet, J. Desbois, C. Monthus, Ann. Phys. **239**, 312 (1995).